Submitted to the Editor of the Astrophysical Journal Letters

Accretion Processes in the Nucleus of M31

Siming Liu[1] and Fulvio Melia[1,2,3]

[1]Physics Department, The University of Arizona, Tucson, AZ 85721

[2]Steward Observatory, The University of Arizona, Tucson, AZ 85721

Received _____; accepted _____

[3]Sir Thomas Lyle Fellow and Miegunyah Fellow.

ABSTRACT

The hypothesized supermassive black hole in the nucleus of M31 (which we shall hereafter call M31*) has many features in common with Sgr A* at the Galactic Center, yet they differ in several significant and important ways. Though M31* is probably ten times heavier, its radio luminosity at 3.6 cm is only one third that of Sgr A*. At the same time, M31* is apparently thousands of times more luminous in X-rays than its Galactic Center counterpart. Thus, a comparative study of these objects can be valuable in helping us to understand the underlying physical basis for their activity. We show here that the accretion model being developed for Sgr A* comprises two branches of solutions, distinguished by the relative importance of cooling compared to compressional heating at the radius r_C where the ambient gas is captured by the black hole. For typical conditions in the ISM, the initial temperature ($T[r_C] \sim 10^6 - 10^7$ K) sits on the unstable branch of the cooling function. Depending on the actual value of $T(r_C)$ and the accretion rate, the plasma settles either onto a hot branch (attaining a temperature as high as $10^{10}K$ or so at small radii) or a cold branch, in which T drops to $\sim 10^4$ K. Sgr A* is presumably a 'hot' black hole. We show here that the VLA, UV and *Chandra* observations of M31* reveal it to be a member of the 'cold' black hole family. We discuss several predicted features in the spectrum of M31* that may be testable by future multi-wavelength observations, including the presence of a prominent UV spike (from hydrogen line emission) that would be absent on the hot branch.

Subject headings: accretion—black hole physics—Galaxy: M31—hydrodynamics—magnetic fields: dynamo—radiation mechanisms: X-rays

1. Introduction

The discovery of an unresolved radio point source (labeled as M31*) in the nucleus of M31 (Crane, Dickel & Cowan 1992) led to an early suggestion (Melia 1992b) that its nature may be similar to that of the supermassive black hole candidate, Sgr A*, at the center of our own Galaxy. The distance to M31 renders its nuclear environment difficult to observe with anything approaching the spatial resolution now available for the Galactic Center, but certain cues suggest that in both cases we may be dealing with a massive pointlike object accreting gas from the interstellar medium, possibly from the winds of stars in the central cluster. However, there do exist several notable differences between the two systems, making a comparative analysis of their emitting regions highly desirable.

The *Hubble Space Telescope* (HST) resolved the nucleus of M31 into two components (P1 and P2) separated by about $0\farcs5 \approx 1.9$ pc (Lauer et al. 1993). The rotational velocity measurements of the stars near the nucleus (Kormendy & Bender 1999) support the idea that this structure is a torus of stars orbiting a central dark, compact object of mass $3.0 \times 10^7\, M_\odot$ in a slightly eccentric trajectory (Tremaine 1995). High resolution ultraviolet images of the nucleus show that there is a group of UV-bright stars between P1 and P2 (Brow et al. 1998), making it very difficult to study the compact object at this frequency. Nonetheless, an HST far-UV observation in 1991 (King, Stanford & Crane 1995) did reveal something peculiar about the region near P2; this source, it appears, has a UV upturn that is much greater than that of the bulge light, while the UV upturn of the optically brighter P1 (which is displaced relative to the dynamical center of the nucleus) is similar to that of its surroundings. These authors argue that the FUV flux level ($\sim 3\mu$Jy) from P2 is not likely to come from stars, but is rather a high-frequency extension of the radio source M31*.

In the radio, there now exist measurements of M31*'s flux at two epochs (Crane et al. 1992; Crane et al. 1993), showing that, at least at 3.6 cm, its luminosity is variable on a time scale of a year or less. But even though M31* is apparently ten times more massive than the black hole at the Galactic Center, its power at 3.6 cm is only one third that of Sgr A* (assuming a distance to M31 of 784 kpc; Stanek & Garnavich 1998). This contrasts with the situation at higher energy,

where M31* is apparently thousands of times more luminous than the latter in X-rays (Garcia et al. 2000). The recent *Chandra* observation also shows that M31* has an extremely soft X-ray spectrum, while the X-ray spectrum of Sgr A* is much harder (Baganoff et al. 2000).

The recent modelling of Sgr A* (Melia, Liu & Coker 2000a, 2000b), taking into account the latest high precision mm, sub-mm and *Chandra* measurements, suggests that (at least in this source) the rate of accretion ($\dot{M}$) toward small radii ($< 30\, r_S$, where r_S is the Schwarzschild radius $\equiv 2GM/c^2$) must be significantly smaller than the rate of wind capture at the Bondi-Hoyle radius $r_C \equiv 2GM/v_\infty^2$, where v_∞ is the velocity of the ambient gas flowing past the central object. Hydrodynamic simulations of the environment surrounding Sgr A* indicate that the infalling gas circularizes when it approaches within $5 - 25\, r_S$ of the black hole. The sub-mm "excess" emission seen in the spectrum of this source appears to be associated with radiation produced within the inner Keplerian region. This view is supported by the linear polarization observed in Sgr A* at mm and sub-mm wavelengths (Aitken et al. 2000), which is difficult to reconcile with other geometries of the emitting region. Both the degree of polarization and the rotation (by about 90°) in the position angle appear to be consistent with a transition of the emitting region within the Keplerian flow from optically thick emission (at mm and longer wavelengths) to optically thin emission in the sub-mm range (Melia 1992a; 1994). The overall spectrum from this region includes a high-energy component due to bremsstrahlung and inverse Compton scattering processes, which may account for the *Chandra* X-ray source coincident with Sgr A* if it turns out to be the actual counterpart to this object (Baganoff et al. 2000).

The situation in the nucleus of M31 may be quite different for several reasons. First, v_∞ around Sgr A* may be anomously high due to the presence of strong wind-producing young stars. In M31, on the other hand, very little is known about the nuclear gas motion, although on a larger scale, Rubin & Ford (1971) find that the plasma within the inner 400 pc region shows a complex velocity field superposed on the rapid rotation, with evidence for expansion at velocities up to ~ 100 km s^{-1}. Second, the central stellar distribution, as noted above, is clearly anisotropic, with P2 lying a mere $2.5 \times 10^5\, r_S$ away from the central black hole. In M31, a lower v_∞, together with

the disruption to the gas flow caused by these stars, may result in a greater accretion rate with a smaller specific angular momentum.

It is well known that the gas temperature near the capture radius is dependent upon the kinetic energy flux brought into this region by the pre-shocked wind. An important consequence of a weaker wind is an initial gas temperature T as low as 10^6 K at large radii, compared with a value as high as 10^7 K in the Galactic Center. A thin plasma under these conditions sits on the unstable branch of the cooling function (Gehrels & Williams 1993). As it continues to fall inwards toward the accretor, it can either heat up to 10^{10} K or more, at which point the cooling rate balances heating, or it cools down to several times 10^4 K, where the energy loss rate drops precipitously. In general, a lower initial temperature and a larger particle number density force the plasma into the lower T stable branch while the higher T branch is favored by the gas starting its descent with a high T and low density.

In this *Letter*, we explore this dichotomy in accretion profiles, and suggest that Sgr A* may represent the hot branch, while M31* may very well be a member of the cold branch family of accreting black holes. In both cases, the initial temperature near the capture radius falls within the unstable region, but as we shall see, M31* appears to be accreting at a higher rate than Sgr A*. If indeed the plasma in M31* is stabilized at about 1.5×10^4 K toward smaller radii, its FUV spectrum should be characterized by strong hydrogen line emission, while its soft X-ray emission is produced by recombination in the hot outer region. This is in contrast with Sgr A*, where our current understanding is that the X-rays are produced by the hot gas within the compact mm and sub-mm emitting gas. We emphasize that our analysis and conclusions regarding M31* are based on the assumption that both the 3.6 cm and *Chandra* measurements represent the actual source strength, rather than upper limits due to the possible contamination by diffuse emission. One of our goals is to make available several testable predictions for the next generation of coordinated observations.

2. Spectral Data for the Nucleus of M31

We collect here the currently available spectral measurements for the nuclear region in M31. M31* was observed in the radio at 3.6 cm in 1990 and 1992 using the VLA in the A configuration (Crane et al. 1992 & 1993). The angular resolution for the two observations was $0\farcs42 \times 0\farcs31$ and $0\farcs29 \times 0\farcs26$, respectively, which are sufficient to attribute the observed flux to a single point source. The measured flux densities differ by about 30% between the two epochs, suggesting a strong variability in M31*. Its luminosity is about one-third that of Sgr A*, itself a variable radio point source at the Galatic Center, with a flux density at 3.6 cm of ≈ 0.7 Jy (Falcke et al. 1998). The measurements at other radio wavelengths (Hjellming & Smarr 1982) provide only upper limits to M31*'s spectrum due to their relatively poor spatial resolution.

The angular resolution for all the available observations between infrared and ultraviolet is also rather poor. The IRAS observations cover a region of $2\farcm0 \times 2\farcm0$, which is about $0.21\,\mathrm{kpc}^2$ at the distance to M31, while the optical to ultraviolet observations at KPNO cover the whole galaxy. The FOC (on *HST*) observations of M31* are hampered by contamination from the blue stars around the center (Brown et al. 1998), so these too should be considered as upper limits. However, the 0.175μm point represents the flux from this region once the contribution from these stars has been subtracted out (King et al. 1995).

With a spatial resolution of $0\farcs8$, *Chandra* was able to resolve the nucleus of M31 into five point sources (Garcia et al. 2000). Although one of these, CXO J0042442.2+411609, is only $1\farcs2$ away from the suspected counterpart to M31*, its contamination can still be limited, and the value quoted in the table should be that of the nuclear source only. Unfortunately the photon statistics above 1.5 keV are rather poor, so the flux measurement in the $1.5 - 7.0$ keV band should be viewed as an upper limit only. Garcia et al. (2000) infer that the X-ray source is strongly variable, when the recent data are compared to earlier *Einstein* observations of the TF 56 source (Trinchieri & Fabbiano 1991).

λ or Energy band	ν (Hz)	F_ν (Jy)	Diameter	Telescope or Intrument	Date	Notes
3.6cm	8.4×10^9	$(28 \pm 5) \times 10^{-6}$	$0\farcs42 \times 0\farcs31$	VLA	June 1990	1
3.6cm	8.4×10^9	$(39 \pm 5) \times 10^{-6}$	$0\farcs29 \times 0\farcs26$	VLA	Nov 1992	2
100μm	3.0×10^{12}	12.0	$2\farcm0 \times 2\farcm0$	IRAS	1983	3,4
60μm	5.0×10^{12}	7.1	$2\farcm0 \times 2\farcm0$	IRAS	1983	3,4
25μm	1.2×10^{13}	0.91	$2\farcm0 \times 2\farcm0$	IRAS	1983	3,4
12μm	2.5×10^{13}	1.83	$2\farcm0 \times 2\farcm0$	IRAS	1983	3,4
0.75μm	4.0×10^{14}	0.746	$190' \times 60'$	0.9m(KPNO)	Sep 1991	5
0.61μm	5.0×10^{14}	0.417	$190' \times 60'$	0.9m(KPNO)	Sep 1991	5
0.53μm	5.6×10^{14}	0.278	$190' \times 60'$	0.9m(KPNO)	Sep 1991	5
0.46μm	6.5×10^{14}	0.177	$190' \times 60'$	0.9m(KPNO)	Sep 1991	5
0.40μm	7.5×10^{14}	0.075	$190' \times 60'$	0.9m(KPNO)	Sep 1991	5
0.35μm	8.6×10^{14}	0.024	$190' \times 60'$	0.9m(KPNO)	Sep 1991	5
0.280μm	1.1×10^{15}	4.85×10^{-4}	$2\farcs8 \times 2\farcs8$	FOC on HST	Feb 1994	6
0.199μm	1.5×10^{15}	2.47×10^{-4}	$2\farcs8 \times 2\farcs8$	FOC on HST	Feb 1994	6
0.175μm	1.7×10^{15}	6.7×10^{-6}	$0\farcs5 \times 0\farcs5$	FOC on HST	1991	7
0.3-1.5keV	$(0.7 - 3.6) \times 10^{17}$	1.8×10^{-7}	$2\farcs0 \times 2\farcs0$	Chandra	Oct 1999	8
1.5-7.0keV	$(0.4 - 1.7) \times 10^{18}$	7.8×10^{-10}	$2\farcs0 \times 2\farcs0$	Chandra	Oct 1999	8

Notes: (1) Crane, Dickel & Cowan. 1992. (2) Crane et al. 1993. (3) Soifer et al. 1986. (4) Neugebauer et al. 1984. (5) Mcquade, Calzetti & Kinney 1995. (6) Brow et al. 1998. (7) King, Stanford & Crane. 1995. (8) Garcia et al. 2000.

3. Accretion from the Ambient Medium and Calculation of the Spectrum

A direct application of the Sgr A* accretion model (e.g., Coker & Melia 2000; Melia, Liu & Coker 2000b) to M31* immediately runs into problems because of the large disparity between the radio to X-ray flux ratios of these two sources. The spectrum of M31* simply does not support

the idea that the inflowing gas is hot ($\sim 10^{10}$ K or so) at small radii. We have therefore explored the characteristics of the accretion model in the high-$\dot{M}$ context to gauge the importance of rapid cooling in this environment. (The motivation for suspecting a higher $\dot{M}$ here than for Sgr A* is based on the factors described in § 1 above.)

The relativistic black hole accretion model was pioneered by Shapiro (1973), and later developed more fully by several workers, the more recent of whom applied this picture to Sgr A* (e.g., Melia 1992a, 1994). Our calculation of the accretion profile for M31* follows the prescription of Coker & Melia (2000), though with several important differences. First, we will restrict our attention to the cold branch solutions for which the impact of a magnetic field B is negligible. Thus, it is not important here to worry about an empirical fit for B. Second, we are in a domain where cooling dominates the energy equation, especially at large radii where the conditions warrant a careful treatment of line cooling (Gehrels & Williams 1993). Thus, whereas this effect could be ignored in the case of Sgr A*, we must include it here, and for this we adopt the cooling function used by these authors, corresponding to a thin gas with cosmic abundances.

Without a specific determination of the gas conditions within a parsec or so of M31*, we are compelled to treat the gas kinematics as an unknown. We therefore adopt a fiducial wind velocity v_∞ of 500 km s^{-1}. In the cold branch solutions, a lower value of v_∞ simply cools the gas faster because $\dot{M}$ is higher. The corresponding Bondi-Hoyle capture radius for M31* is then $r_C = 3.6 \times 10^5 r_S$, which by the way, is larger than the distance from M31* to P2 (see above). With M and v_∞ known, the accretion rate then depends on the gas density, which unfortunately is also poorly constrained. However, Ciardullo et al. (1988) argue that the ionized-gas density gradient in the nucleus of M31 is dramatic, dropping from $n_e \sim 10^4$ electrons cm^{-3} at a radius of $\sim 7''$ to 10^2 electrons cm^{-3} at $\sim 1'$. Thus, simply putting $\dot{M} \sim \pi r_C^2\, m_p n_e\, v_\infty$, where m_p is the proton mass, and $n_e = 10^4$ cm^{-3}, we see that $\dot{M}$ may be as high 10^{25} g s^{-1}.

The temperature at the outer boundary ($\sim r_C$) is estimated by assuming that the kinetic

energy in the gas is thermalized by shocks, for which

$$2R_gT(r_C) \sim \frac{1}{2}\left(\frac{3}{4}v_\infty\right)^2, \tag{1}$$

where R_g is the gas constant. Since magnetic heating is negligible at large radii, we neglect its effect for the following discussion. Then, the principal radiating mechanisms are radiative recombination, and thermal bremsstrahlung emission. Electron-positron pair production and Comptonization are both negligible due to the low temperature we have in the cold branch solutions. For simplicity, we here consider only hydrogen recombination to calculate the line emission. A more sophisticated treatment that includes the contribution from all the ions will be discussed elsewhere. For this, the ionization fraction may be calculated according to the prescription given in Rossi et al. (1997).

4. Results and Conclusions

The principal distinguishing feature between the hot and cold branch solutions is illustrated in Figure 1, which shows the temperature profile of the accreting gas as a function of radius. The emphasis here is the dependence of this profile on the initial temperature, so all the other physical conditions are identical for the three cases included on this plot, and are based on the best fit model for the spectrum of M31* (dark, solid curve). In all cases, the outer boundary is taken to be $r_0 = 10^5\, r_S$, with an accretion rate $\dot{M} = 1.5 \times 10^{24}$ g s^{-1}. The ratio of thermal to gravitational energy density at r_0, which characterizes the initial temperature, is 1/57, 1/59 and 1/88, respectively, for the thin, solid curve (the sole hot branch solution), the thick, solid curve (the best fit model), and the dotted curve. For the reasons discussed in the previous section, lowering $\dot{M}$ has the effect of moving the transition temperature between the hot and cold branches to lower values. Thus, with an appreciably lower $\dot{M}$, Sgr A* lies comfortably within the category of hot branch solutions since its initial temperature appears to be larger than that of M31* (at $\sim 2 \times 10^6$ K). For the massive black hole in M31, however, the gas cools quickly as it collapses towards smaller radii, and has reached the cold, stable branch of the cooling curve (at $\sim 10^4$ K)

by the time it crosses $\sim 10^4\, r_S$. Thereafter, the heating due to compression (for this particular set of parameters) never quite catches up and the gas continues to radiate efficiently as it plummets toward the event horizon.

The spectrum produced by this plasma is shown in Figure 2 (dark, solid curve), in which we have also indicated the contribution from the hot ($T > 10^6$ K), outer region (thin, solid curve), and the cooler ($T < 10^6$ K), inner zone (dotted curve). The transition radius between these two domains is approximately $10^4\, r_S$ (see Fig. 1). The most constraining data on this plot are the VLA measurements (Crane et al. 1992; Crane et al. 1993), the FUV point inferred from the subtraction of starlight (King et al. 1995), and the more recent *Chandra* results (shown as a butterfly below 1.5 keV and as an upper limit above this energy; Garcia et al. 2000). We see that the X-rays are produced in the outer, hot region, whereas the FUV spike arises from hydrogen line emission, predominantly in the cooler, inner zone. The radio portion of the spectrum is produced throughout the accretion volume.

We would thus expect M31*'s X-ray flux to vary on a time scale $\tau \sim 10^4\, r_S/v_{ff} \leq 7$ years, where the free-fall velocity v_{ff} at $10^4\, r_S$ is approximately $c/100$. Its radio flux, which is produced throughout the volume of captured gas, should also vary on a time scale no larger than this, though only a portion of this variability is expected to be correlated with the X-rays. Since some of the radio emission occurs at smaller radii, we expect that relative to the X-rays, the 3.6 cm emission ought to display variability with a broader range of time scales.

Figure 2 also highlights one of the main features that distinguish the spectra of the hot and cold solutions—the FUV spike due to line emission, which is absent in the former, but is very prominent in the latter. This may be the origin of the peculiar UV upturn near P2 noted by King et al. (1995) in their analysis of the non-stellar contribution to the UV flux. The strength of this spectral component suggests that additional UV observations of the region near P2 are called for. The variability in the UV flux may be more tightly correlated with that at 3.6 cm, rather than the X-rays, though the UV emissivity at $r > 10^4\, r_S$ is not insignificant.

In calculating the spectrum for the hot branch solution of Figure 1, we have not included the

effects due to a magnetic dynamo, should the gas circularize before it reaches the event horizon. In the case of Sgr A*, the dominant contribution to the mm and sub-mm spectrum is made by a Keplerian structure within the inner $5\,r_S$ or so (Melia, Liu & Coker 2000a, 2000b). In the case of M31*, this region may or may not exist, depending on how much specific angular momentum is carried inwards. For the same conditions as in Sgr A*, M31* would not have a Keplerian region (and hence a magnetic dynamo to produce the sub-mm bump) since $r_S(M31*) \approx 10\,r_S(SgrA*)$, i.e., the gas would not circularize before crossing the event horizon. The spectrum of the hot branch solution, without a synchrotron component, is shown (with the same line type as in Fig. 1) in Figure 3. Here, most of the X-rays are produced in the hot inner region. This spectrum is not consistent with the data, and if the *Chandra* nuclear source is indeed the counterpart to M31*, we can rule out the hot branch solution for this object. The other cold branch solution (dotted curve in Fig. 1) has a spectrum that is still a reasonable fit to the VLA and UV data, but falls short in X-rays. Future co-ordinated multi-wavelength observations of this intriguing supermassive black hole candidate would be invaluable.

We are indebted to Fred Baganoff, Mike Garcia, Ivan King, and Mark Morris for very valuable discussions and clarifications. This work was supported by a Sir Thomas Lyle Fellowship and a Miegunyah Fellowship for distinguished overseas visitors at the University of Melbourne, and by NASA grants NAG5-8239 and NAG5-9205.

REFERENCES

Aitken, D.K., Greaves, J., Chrysostomou, A., Jenness, T., Holland, W., Hough, J.H., Pierce-Price, D. & Richer, J. 2000, ApJ Letters, 534, L173

Baganoff, F. et al. 2000, ApJ, to be submitted

Brown, T.M., Ferguson, H.C., Stanford, S.A. & Deharveng, J.-M. 1998, ApJ, 504, 113

Ciardullo, R., Rubin, V.C., Jacoby, G.H., Ford, H.C. & Ford, W.K. Jr. 1988, AJ, 95, 438

Coker, R.F. & Melia, F. 1997, ApJ Letters, 488, L149

Crane, P.C., Dickel, J.R. & Cowan, J.J. 1992, ApJ Letters, 390, L9

Crane, P.C., Cowan, J.J., Dickel, J.R. & Roberts, D.A. 1993, ApJ Letters, 417, L61

Falcke, H., Goss, W.M., Matsuo, H., Teuben, P., Zhao, J.-H. & Zylka, R. 1998, ApJ, 499, 731

Gehrels, N. & Williams, E.D. 1993, APJ Letters, 418, 25.

Garcia, M.R., Murray, S.S., Primini, F.A., Forman, W.R., McClintock, J.E. & Jones, C. 2000, ApJ Letters, 537, L23

Hjellming, R.M. & Smarr, L.L. 1982, ApJ Letters, 257, L13

King, I.R., Stanford, S.A. & Crane, P. 1995, AJ, 109, 164

Kormendy, J. & Bender, R. 1999, APJ, 522, 772

Lauer, T.R., et al. 1993, AJ. 106, 1436

Mcquade, K., Calzetti, D. & Kinney, A.L. 1995, ApJS, 97, 331

Melia, F. 1992a, ApJ Letters, 387, L25

Melia, F. 1992b, ApJ Letters, 398, L95

Melia, F. 1994, ApJ, 426, 577

Melia, F., Liu, S. & Coker, R.F. 2000a, ApJ, in press

Melia, F., Liu, S. & Coker, R.F. 2000b, ApJ Letters, in press

Neugebauer, G., Habing, H.J., Duinen, R.V., Aumann, H.H., Baud, B., Beichman, C.A., Beintema, D.A., Boggess, N., Clegg, P.E., Jong, T.De, Emerson, J.P., Gautier, T.N., Gillett, F.C., Harris, S., Hauser, M.G., Houck, J.R., Jennings, R.E., Low, F.J., Marsden, P.L., Miley, G., Olnon, F.M., Pottasch, S.R., Raimond, E., Rowan-Robinson, M., Soifer, B.T., Walker, R.G., Wesselius, P.R. & Young, E. 1984, ApJ Letters, 278, L1

Rossi, P., Bodo, G., Massaglia, S. & Ferrari, A. 1997, AA, 321, 672

Rubin, V. & Ford, W.K. Jr. 1971, ApJ, 170, 25

Shapiro, S.L. 1973, APJ, 180, 531

Soifer, B.T., Rice, W.L., Mould, J.R., Gillett, F.C., Robinson, M.R. & Habing, H.J. 1986, APJ, 304, 651

Stanek, K.Z. & Garnavich, P.M. 1998 ApJ Letters, 503, L131

Tremaine, S. 1995, AJ, 110, 628

Trinchieri, G. & Fabbiano, G. 1991, APJ, 382, 82

This manuscript was prepared with the AAS LaTeX macros v4.0.

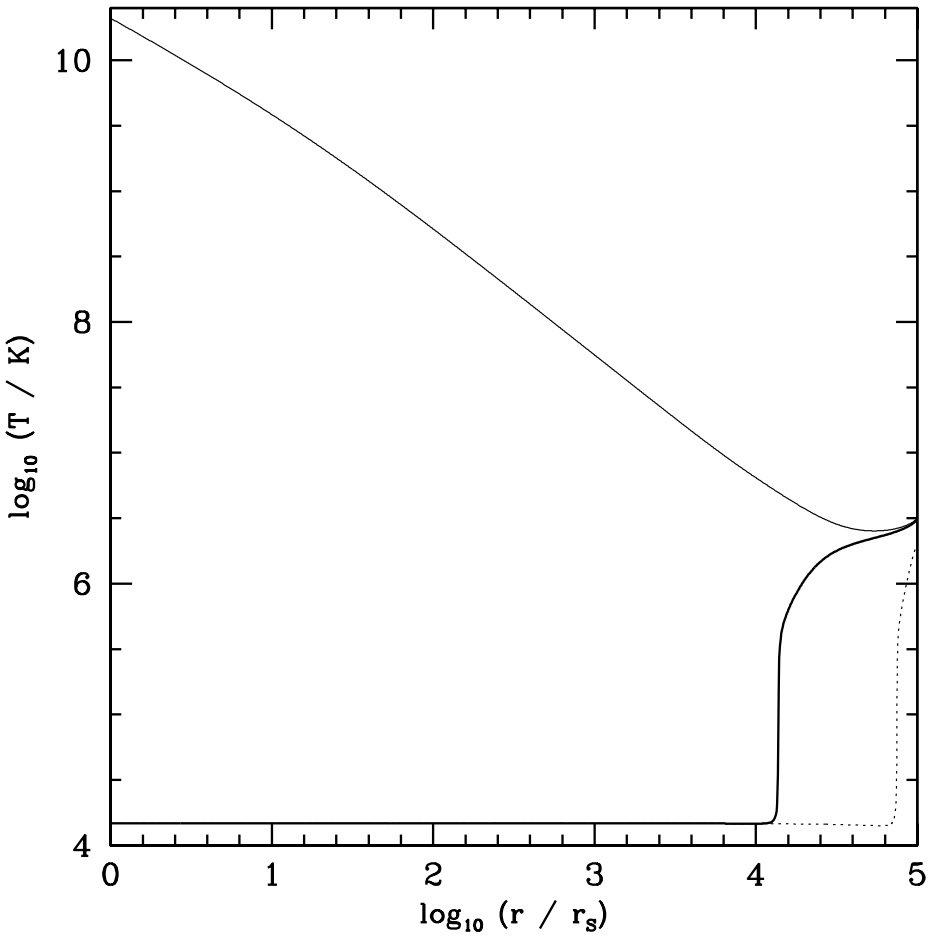

Fig. 1.— Temperature profile for the accreting gas, for three values of the initial temperature at the outer radius $r_0 = 10^5\, r_S$. The accretion rate in all cases is $\dot{M} = 1.3 \times 10^{24}$ g s^{-1}. The initial temperature is characterized by the ratio of thermal to gravitational energy density at r_0, which is 1/57 (thin, solid curve—the hot branch solution), 1/59 (thick, solid curve—the best fit model for M31*) and 1/88 (dotted curve).

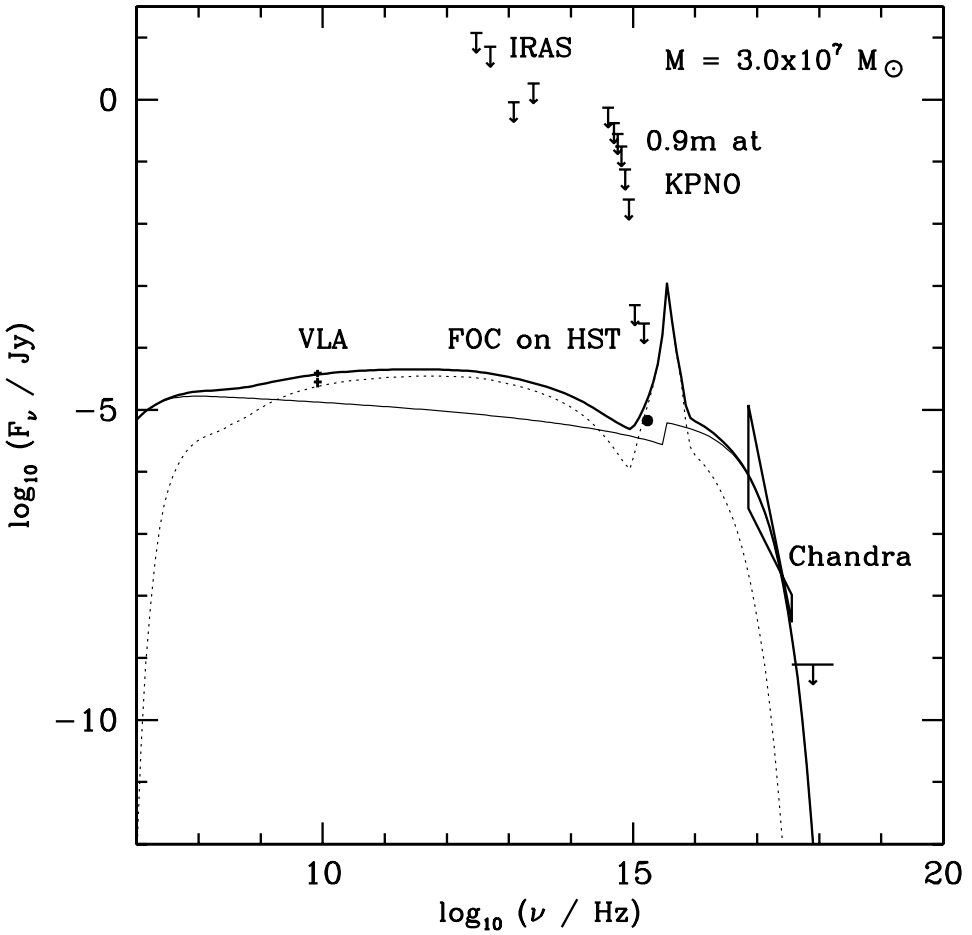

Fig. 2.— Spectrum for the best fit model. The parameter values are specified in the caption of Figure 1. Here, the thin solid curve represents the contribution from the outer hot ($T > 10^6$ K) region, beyond $\sim 10^4\, r_S$. The step in the curve is due to radiative recombination. The dotted curve corresponds to the emissivity from the inner cool region, which accounts for the prominent UV peak due to hydrogen line emission.

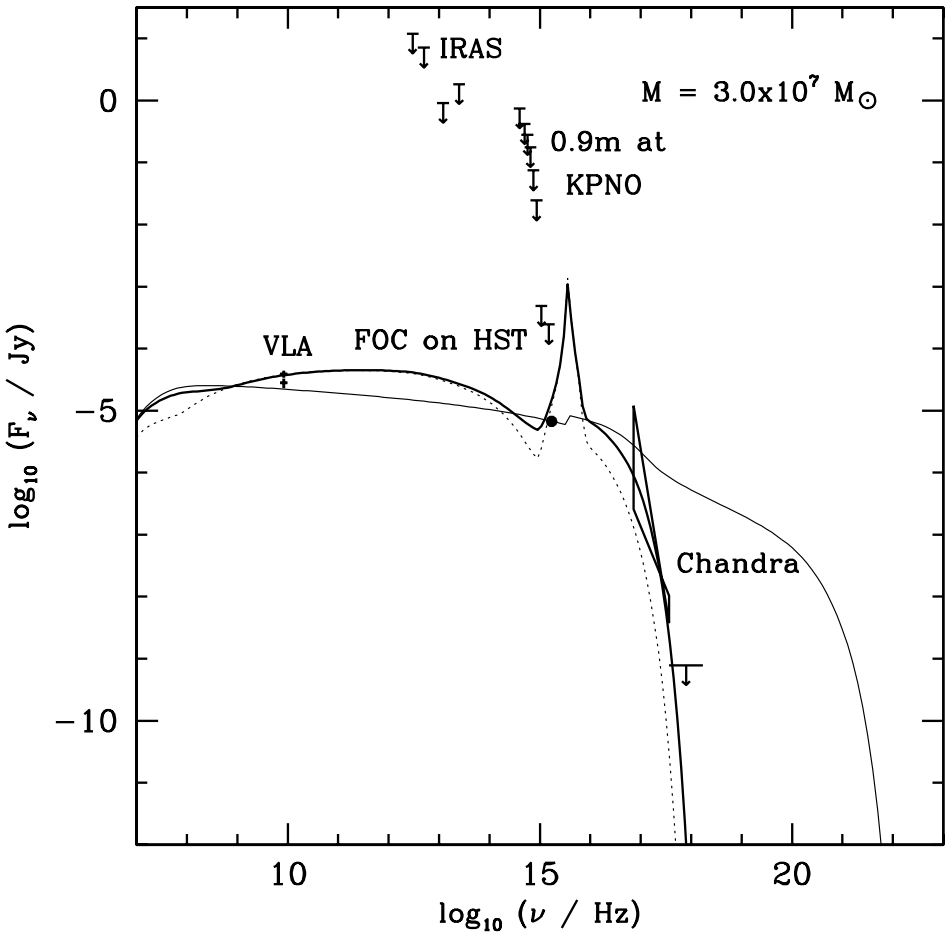

Fig. 3.— A comparison of the overall spectrum arising from each of the three cases depicted in Fig. 1. The line types have the same definitions as those in the first figure.